

Optics Letters

Optimal principal component analysis-based numerical phase aberration compensation method for digital holography

JIASONG SUN,^{1,2,3} QIAN CHEN,^{2,4} YUZHEN ZHANG,² AND CHAO ZUO^{1,2,*}

¹Smart Computational Imaging (SCI) Laboratory, Nanjing University of Science and Technology, Nanjing, Jiangsu Province 210094, China

²Jiangsu Key Laboratory of Spectral Imaging & Intelligent Sense, Nanjing University of Science and Technology, Nanjing, Jiangsu Province 210094, China

³e-mail: sjs0808402013@163.com

⁴e-mail: chenqian@njjust.edu.cn

*Corresponding author: surpasszuo@163.com

Received 24 January 2016; accepted 18 February 2016; posted 22 February 2016 (Doc. ID 258007); published 15 March 2016

In this Letter, an accurate and highly efficient numerical phase aberration compensation method is proposed for digital holographic microscopy. Considering that most parts of the phase aberration resides in the low spatial frequency domain, a Fourier-domain mask is introduced to extract the aberrated frequency components, while rejecting components that are unrelated to the phase aberration estimation. Principal component analysis (PCA) is then performed only on the reduced-sized spectrum, and the aberration terms can be extracted from the first principal component obtained. Finally, by oversampling the reduced-sized aberration terms, the precise phase aberration map is obtained and thus can be compensated by multiplying with its conjugation. Because the phase aberration is estimated from the limited but more relevant raw data, the compensation precision is improved and meanwhile the computation time can be significantly reduced. Experimental results demonstrate that our proposed technique could achieve both high compensating accuracy and robustness compared with other developed compensation methods. © 2016 Optical Society of America

OCIS codes: (090.1995) Digital holography; (090.1000) Aberration compensation; (090.2880) Holographic interferometry; (120.5050) Phase measurement.

<http://dx.doi.org/10.1364/OL.41.001293>

In last decades, digital holographic microscopy (DHM) has become a powerful tool since the development of CCD and CMOS cameras permits the real-time recording of a digital hologram and quantitative retrieval of the complex wavefront of the samples with high accuracy [1]. However, the reconstructed phase images generally suffer from a spherical phase curvature introduced by the microscope objective (MO), which needs to be compensated to access the exact phase induced by the object only [2]. Generally, the spherical phase aberration term, which needs to be compensated, can be written as

$$Q(x, y) = e^{i(k_x x + l_x x^2 + k_y y + l_y y^2)}, \quad (1)$$

where the factors k_x, k_y denote the linear phase difference between the object beam $O(x, y)$ and reference beam $R(x, y)$ due to the off-axis geometry, while the parameters l_x, l_y describe the relative divergence between $O(x, y)$ and $R(x, y)$ due to the mismatch in spherical phase curvature. Once the coefficients of $Q(x, y)$ have been determined, the spherical phase curvature introduced by the MO can be compensated by multiplying with its conjugation Q^* .

Recently, a lot of methods have been proposed to compensate this curvature $Q(x, y)$ of the wavefront in DHM either physically [3–6] or numerically [1, 7–14]. Normally, the spherical phase factor could be physically compensated by introducing the same curvature in the reference arm using a same objective [3] or position adjustable lens [4], or arranging the whole optical geometry in a telecentric manner [6]. However, the phase curvature is difficult to be completely eliminated because a perfect matching between the object and reference wavefront curvatures is difficult to realize in practice. On the other hand, instead of compensating the aberration physically, the numerical methods remove the phase aberration during post processing of the digital hologram. Double exposure method [11] can obtain the curvature $Q(x, y)$ accurately, but an additional hologram recording without the samples is required. Other methods either multiply an adapted phase mask in the reconstruction plane or hologram plane [7, 11], or directly fit the curvature $Q(x, y)$ with a standard two-dimensional (2D) spherical function [10] or Zernike polynomials [12] by using 2D fitting methods. However, these techniques are generally time-consuming, because even for the simplest 2D least-squares surface fitting method [10] the processing time could be several seconds for a typical megapixel hologram while 2D phase unwrapping is required, which limits the real-time performance of DHM. Recently, Zuo proposed a numerical aberration compensation method based on principal component analysis (PCA) by using the singular value decomposition (SVD) [14]. The definition of two one-dimensional (1D)

vectors $p(x) = e^{i(k_x x + l_x x^2)}$ and $q(y) = e^{i(k_y y + l_y y^2)}$ with the phase aberration matrix rewritten as $Q(x, y) = pq^T$ is introduced in Ref. [14] to transfer 2D phase unwrapping and 2D surface fitting problems into 1D procedure on two orthogonal directions, which could improve the compensating efficiency significantly.

Unfortunately, although the computational dimension is reduced from 2D to 1D after PCA, PCA itself could be a time-consuming task because its processing time depends on the size of images. If the PCA algorithm with full-sized complex images is implemented, the SVD process would result in exponential growth of the PCA processing time with the image size increasing, as shown in Fig. 1. Even if the current PCA-based numerical compensation method (cPCA) introduced in Ref. [14] extracts the first principal component from the +1 order spectrum, the PCA procedure could also waste a long time if a larger +1 order spectrum is selected. To ensure its efficiency, one simple way is to limit or reduce the size of the selected +1 order spectrum. However, the amount of high-frequency components would lose in this way and the detail information of the recovered complex image would be lost.

To address this efficiency problem in cPCA, this Letter investigates the characteristic of typical phase aberration spectra and presents a highly efficient compensation method by extracting the reduced-sized aberration spectrum. Figures 2(a)–2(c) show three different phase maps of the same specimens and pixel resolution (1280×960), but suffer from different amounts of aberration. The level of phase aberration is apparently manifested by the density of concentric circles in each phase maps. The +1 order spectra of the three phase maps with a dimension of 144×108 are shown in Figs. 2(d)–2(f), respectively. As can be seen, the sizes of the blue windows in Figs. 2(d)–2(f), in which the most of energy of the aberration is concentrated, expand with the increasing amounts of aberration, suggesting that the size of aberration spectrum only depends on the amount of aberration rather than the size of the entire phase image. This observation has been introduced in Refs. [4,6,9]. In practical conditions, only reduced aberrations are normally introduced. Thus, most of its energy is concentrated in a very limited spatial support around the carrier frequency, like Fig. 2(f). Therefore, we introduce a masking operator that limits the support of +1 order spectrum to the region where aberration energy is concentrated. The masking operator significantly reduces the amount of data involved in the computation, and thus the computational efficiency of the PCA process can be greatly improved. Furthermore, because the limited mask almost embraces the total energy of aberration while the object energy (that spread evenly over the entire +1 order spectrum) is

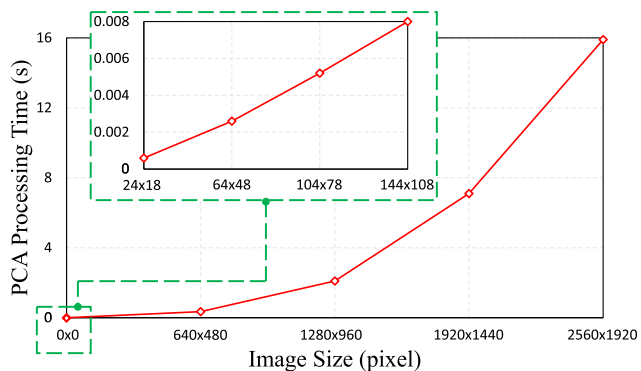


Fig. 1. Curve of PCA processing time increasing with image size.

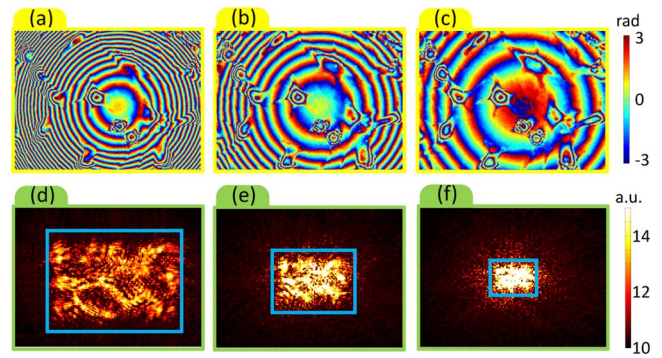


Fig. 2. Comparison of different phase images and their +1 order spectra. (a)–(c) show three phase images of a typical cell sample with different amounts of spherical aberration, respectively; (d)–(f) show their +1 order frequency spectra, respectively.

significantly attenuated, a higher accuracy of phase compensation over cPCA can be expected to be achieved.

Now, the efficiency of the PCA procedure is improved, but the fitting accuracy of the aberration is unexplored. Considering a typical full-sized phase image with spherical aberration shown in Fig. 2(c), its first principal component with resolution of 1280×960 can be extracted through the PCA procedure. One-dimensional vector of the first principal component along X-axis is shown in Fig. 3(a1), and its unwrapped phase distribution (1280 red points) and the fitted parabolic curve (blue curve) is shown in Fig. 3(a2). As can be seen, one red point at the edge of the 1D phase vector is far away from the blue parabolic curve in Fig. 3(a2). Meanwhile, in Fig. 3(a1), this error point at the beginning of the vector has a value that is very close to point at the end of the vector. This inspiring observation reminds us that the spectrum masking procedure can be decomposed into two steps, frequency filtering and under-sampling. It is known that by employing Fourier transform (FT), the filtering process in the frequency domain can be regarded as a cyclic convolution operation in the spatial domain. Therefore, the error point at the beginning of this vector, which has a value averaged by the point at the end of this vector, should be removed before least-squares fitting. However, because there are 1280 points in this vector totally, the fitting accuracy of full-sized phase image is rarely

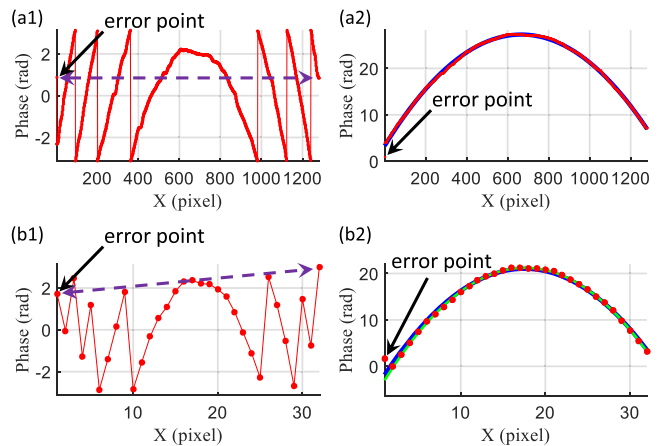


Fig. 3. Wrapped and unwrapped 1D phase vectors along the X-axis obtained from the PCA process with different sizes of selected aberration spectra.

affected by the single error point. Next, considering the reduced-sized aberration spectrum extracted from the blue window in Fig. 2(f), a subsampled (32×24) phase image [Fig. 4(g)] can be obtained through inverse FT and its reduced-sized first principal component [Fig. 4(h)] can be extracted through the PCA procedure. Similarly, a subsampled 1D vector along X-axis is shown in Fig. 3(b1), and its unwrapped phase distribution (32 red points) and the fitted parabolic curve (blue curve) are shown in Fig. 3(b2). It also can be seen that an error point is far away from the blue parabolic curve, which could be removed by setting a reasonable threshold T (typically $T = \frac{\pi}{2}$). After removing the error point, the fitted parabolic curve [green curve in Fig. 3(b2)] is corrected obviously because this vector only involves 32 points. Because the subsampled phase vectors have been corrected, the full-sized phase vectors can be obtained accurately by oversampling.

So, based on these facts, we propose an optimal PCA-based (OPCA) numerical phase aberration compensation method for digital holography. In order to explain the entire framework of OPCA, a set of experimental results of human macrophage cells at the output of each step is presented in Fig. 4. At the beginning of OPCA, the frequency spectrum [Fig. 4(b)] of the digital hologram [Fig. 4(a)] and the cropped +1 order spectrum in Fig. 4(c) are obtained successively. Then the full-sized phase image with aberration [Fig. 4(e)] can be generated through FT

after centering the +1 order spectrum [Fig. 4(d)]. Instead of fitting the full-sized phase aberration image directly, we introduce a masking operator to extract the aberration spectrum [Fig. 4(f)] where aberration energy is concentrated. In OPCA, we select the aberration spectrum in the +1 order spectrum manually, ensuring the aberration spectrum containing more than 80% energy of the +1 order spectrum. Next, after inverse FT, the subsampled phase map with aberration is obtained [Fig. 4(g)]. Utilizing the PCA algorithm and the 1D phase unwrapping technique, the first principle component [Fig. 4(h)] and two unwrapped phase vectors are extracted successively. Figure 4(i) presents one unwrapped phase vector along the X-axis. Different from cPCA, one error point at the edge of each 1D unwrapped phase vector is removed before least-squares fitting in OPCA to improve the fitting accuracy. After getting the corrected parabolic equations [Fig. 4(j)] from those two phase vectors, we employ an oversampling process to avoid the Ringing effect resulted from spectrum truncation. At last, the full-sized phase aberration map [Fig. 4(k)] with dimension 1280×960 can be reconstructed according to Eq. (1) and the compensated phase image [Fig. 4(l)] is finally obtained.

In order to evaluate the improvement of our proposed OPCA phase aberration compensation algorithm, we have applied other different PCA algorithms to the same digital hologram and Fig. 5 shows their compensation results. The ideal reconstructed phase aberration shown in Fig. 5(a) is extracted from the full-sized phase map [Fig. 4(e)] utilizing conventional PCA algorithm after error points removing operation. Although the spherical aberration is compensated accurately, over 2 s are wasted on the SVD process. Figure 5(e) presents the difference in image between Fig. 4(k) and Fig. 5(a), demonstrating that OPCA method truly improves compensating efficiency without sacrificing any compensation accuracy. Moreover, OPCA finishes its PCA process with only 0.001 s. By employing the cPCA algorithm, the reconstructed phase aberration map is presented in Fig. 5(b). This result is obtained from the +1 order spectrum with dimension 144×108 , without removing error

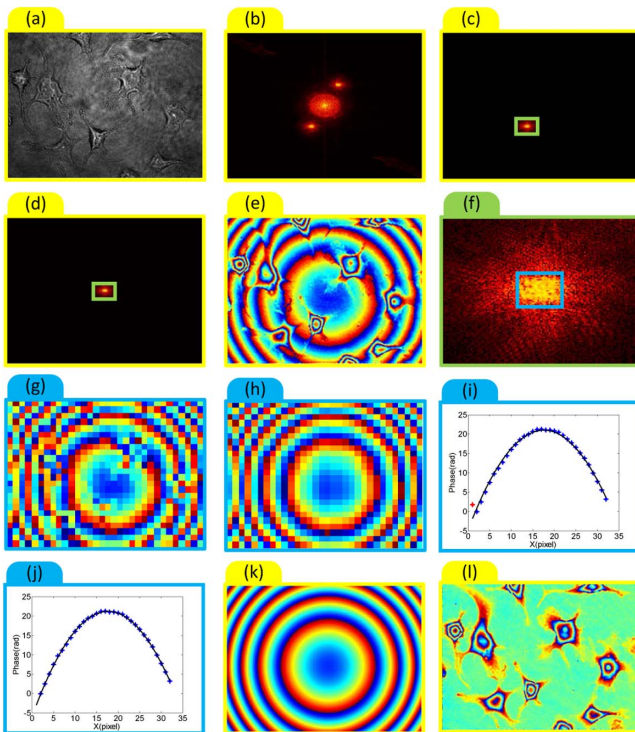
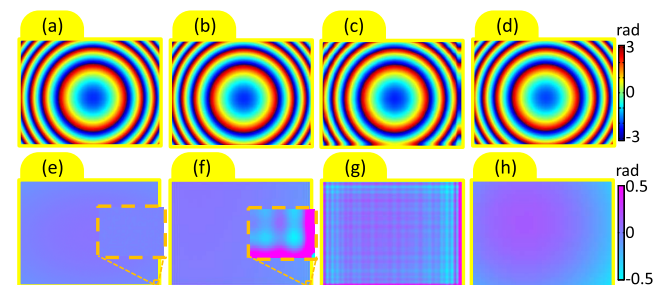


Fig. 4. Experimental results of human macrophage cells at the output of each step in OPCA. (a) Digital hologram; (b) presents the frequency spectrum of (a); (c) shows the cropped +1 order spectrum; (d) presents the centered +1 order spectrum; (e) is the phase image with aberration; (f) presents the cropped aberration spectrum; (g) shows the subsampled phase map; (h) is the extracted first principle component; (i) presents the unwrapped phase vector along the X-axis; (j) shows the fitted curve after error point removing; (k) is the fitted phase aberration map; and (l) is the compensated phase image.



Compensation method	Processing time in PCA (s)	RMSE of recovered phase map (rad)
Full-sized PCA	2.1	0
cPCA in [12]	0.008	0.0686
OPCA without over-sampling	0.001	0.1180
OPCA without error points removing	0.001	0.1320
OPCA	0.001	0.0115

Fig. 5. Performance comparison of five different PCA algorithms.

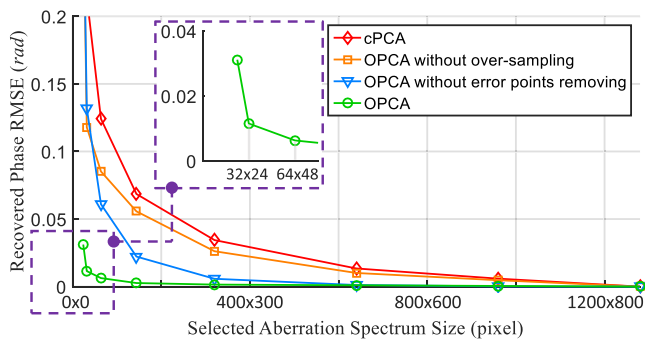


Fig. 6. Accuracy comparison of four different PCA algorithms with different size of selected aberration spectrum.

points and oversampling two phase vectors. Although the result seems similar to the correct phase aberration [Fig. 5(a)], the processing time spent on PCA is 0.008 s, and the processing time would also increase undoubtedly with a larger +1 order spectrum. Furthermore, noticing the enlargement part in the phase difference map Fig. 5(f), Ringing effect emerges due to the spectrum truncation at the edge of the +1 order spectrum. Figure 5(c) shows the reconstructed phase aberration by employing OPCA method without oversampling. With the limited size of the aberration spectrum, serious Ringing effect occurs in the phase difference map Fig. 5(g) due to the spectrum truncation at the edge of the frequency mask. By employing the OPCA method without error points removing process, the phase aberration cannot be fitted accurately [Fig. 5(d)], leaving residual spherical aberration in the phase difference map as expected [Fig. 5(h)]. Figure 5(i) summarizes the comparison of these five different phase aberration compensation algorithms, which highlights the advantage of our OPCA method in both efficiency and accuracy.

Furthermore, to quantitatively illustrate the relationship between the compensating accuracy and the size of the aberration spectrum, four compensation methods are implemented with different sizes of selected aberration spectrum. Figure 6 presents the root-mean-squared error (RMSE) of the recovered phase images. As can be seen, the cPCA technique is obviously affected by the size of selected aberration spectrum because the error points and the spectrum truncation have not been addressed properly. On the other hand, among these four methods, OPCA achieves the highest compensating accuracy and the best robustness with the frequency mask shrinking. Noticing that the recovered phase RMSE increases rapidly using OPCA when the size of the aberration spectrum reduces to 24×18 , this is because the frequency mask is shrunk smaller than the aberration spectrum. Therefore, the whole aberration spectrum should be selected manually in OPCA to prevent the occurrence of this incorrect compensation.

In conclusion, we have proposed a high-efficiency PCA-based phase aberration compensation method for digital holographic microscopy by introducing a masking operator on the +1 order spectrum to extract the aberration spectrum where aberration energy is concentrated. Because the size of the subsampled aberration spectrum is limited by the masking operator, the computational efficiency of the PCA process is significantly improved. Moreover, the limited mask almost embraces the total energy of aberration while the object energy is significantly attenuated; thus, higher compensation accuracy and robustness are achieved as demonstrated by the experimental results. Based on the PCA technique, when the phase aberration function $Q(x, y)$ only contains non-cross terms and can be separated into two 1D vectors, our method can be further extended to correct some high-order phase aberrations, not just limited to tilt and defocus.

Funding. National Natural Science Foundation of China (NSFC) (11574152, 61505081); ‘Six Talent Peaks’ project (2015-DZXX-009); ‘333 Engineering’ research project (BRA2015294); Fundamental Research Funds for the Central Universities (30915011318); Open Research Fund of Jiangsu Key Laboratory of Spectral Imaging & Intelligent Sense (3092014012200417).

Acknowledgment. The authors thank the Zijin Star program of Nanjing University of Science and Technology for their support.

REFERENCES

1. E. Cucho, P. Marquet, and C. Depeursinge, *Appl. Opt.* **38**, 6994 (1999).
2. W. Zhou, Y. Yu, and A. Asundi, *Opt. Lasers Eng.* **47**, 264 (2009).
3. C. Mann, L. Yu, C.-M. Lo, and M. Kim, *Opt. Express* **13**, 8693 (2005).
4. W. Qu, C. O. Choo, V. R. Singh, Y. Yu, and A. Asundi, *J. Opt. Soc. Am. A* **26**, 2005 (2009).
5. W. Qu, Y. Yu, C. O. Choo, and A. Asundi, *Opt. Lett.* **34**, 3809 (2009).
6. E. Sánchez-Ortiga, P. Ferraro, M. Martínez-Corral, G. Saavedra, and A. Doblas, *J. Opt. Soc. Am. A* **28**, 1410 (2011).
7. T. Colomb, E. Cucho, F. Charrière, J. Kühn, N. Aspert, F. Montfort, P. Marquet, and C. Depeursinge, *Appl. Opt.* **45**, 851 (2006).
8. F. Montfort, T. Colomb, F. Charrière, J. Kühn, P. Marquet, E. Cucho, S. Herminjard, and C. Depeursinge, *Appl. Opt.* **45**, 8209 (2006).
9. T. Colomb, J. Kühn, F. Charrière, C. Depeursinge, P. Marquet, and N. Aspert, *Opt. Express* **14**, 4300 (2006).
10. J. Di, J. Zhao, W. Sun, H. Jiang, and X. Yan, *Opt. Commun.* **282**, 3873 (2009).
11. P. Ferraro, S. De Nicola, A. Finizio, G. Coppola, S. Grilli, C. Magro, and G. Pierattini, *Appl. Opt.* **42**, 1938 (2003).
12. L. Miccio, D. Alfieri, S. Grilli, P. Ferraro, A. Finizio, L. De Petrocellis, and S. Nicola, *Appl. Phys. Lett.* **90**, 041104 (2007).
13. K. W. Seo, Y. S. Choi, E. S. Seo, and S. J. Lee, *Opt. Lett.* **37**, 4976 (2012).
14. C. Zuo, Q. Chen, W. Qu, and A. Asundi, *Opt. Lett.* **38**, 1724 (2013).